Facile synthesis of oxygen doped carbon nitride hollow microsphere for photocatalysis

Yuxiong Wang [a], Hao Wang [a], Fangyan Chen [a], Fu Cao [a], Xiaohua Zhao [b], Sugang Meng [c], Yanjuan Cui [a],*

[a] School of Environmental and Chemical Engineering, Jiangsu University of Science and Technology, Zhenjiang 212003, PR China
[b] School of Materials Science and Engineering, Jiangsu University, Zhenjiang 212013, PR China
[c] Department of Chemistry, Huaibei Normal University, Anhui, Huaibei 235000, PR China

ARTICLE INFO

ABSTRACT

Tailoring defective conjugated heterocyclic network to make for broaden light absorption and efficient charge separation for photocatalytic application is an urgent assignment for graphitic carbon nitride (g-C_3N_4) materials. Here we report a ficile "one-pot" solvothermal method to synthesize controllable O-doped g-C_3N_4 catalysts at low temperature. By this template-free approach, hollow microsphere O-doped g-C_3N_4 products were obtained. Structure characterization reveals that the as-prepared sample has incomplete heptazine heterocyclic ring structure, and appears O doping in the lattice, which may derived from the activated O_2 molecular. With the extending condensation time, the increased heteroelement doping content and narrowed band gap promote the light harvesting and charge separation efficiency. Compared to pristine g-C_3N_4 prepared under high-temperature calcination, this novel material show remarkably photocatalytic activity for environment pollutant purification and splitting water for H_2 evolution, even though the conduction level decrease. This work highlights that the architecture and electronic properties of g-C_3N_4 based materials could be facile control through mild solvothermal route, which is a reference way for design and fabricate highly efficient non-metal photocatalyst with peculiar feature.

© 2017 Elsevier B.V. All rights reserved.

1. Introduction

Semiconductor-mediated photocatalysis technology has been regarded to be the most appealing methods for environmental pollutant elimination and energy transformation, like degradation of organic pollutants and splitting water to produce hydrogen [1–3]. At present, hundreds of functional materials using as photocatalysts have been developed, such as so many metal oxides, nitrides, sulphides and so on [4–6]. However, the extensive application of photocatalysis in practice still faces huge changes due to the poor quantum conversion efficiency, expensive raw materials and activity unstability.

Nowadays, more reaches tend to focus on metal-free catalytic/photocatalytic material, because of its unique advances, such as rich raw material, plenty of modification feasibility, and environmentally friendly. In recent years, binary carbon nitrides (CNs), one of the oldest metal-free polymer, has been regarded as promising

novel green photocatalysts with visible light. Since 2009, g-C_3N_4 was reported by Wang et al. as an attractive photocatalyst for producing hydrogen from water, the application of this catalyst has been expanded to several fields, like sensors, artificial light synthesis, CO_2 reduction, etc. [7–12] In order to overcome the inherent restrict of intrinsic carbon nitride materials, so many reach works focus on modification of g-C_3N_4 to optimize its structure so that to enhance its photocatalytic properties have been done. Up to now, g-C_3N_4 with diverse nanostructures and morphology obtained from replication of hard templates has been reported. For example, g-C_3N_4 nanorods and mesoporous spheres used as photocatalysts for hydrogen generation have been successfully synthesized from template-induced method (silicon or molecular sieve) [13–16]. Even so, the complicated synthetic procedures and indispensable corrosive reagent (HF, NH_4HF_2, etc.) brings the possible risk for preparation and environment. In composition to hard-templating, soft templates make the synthesis process simple and the morphological tuning diversiform. Therefore, soft templating method is more desirable alternation. For many researchers, bubble templating method using urea or thiourea as sacrifice reagent have been reported to obtain porous g-C_3N_4 [17,18]. However, there are few

* Corresponding author.
  E-mail addresses: yjcui@just.edu.cn, ganlan.s@163.com (Y. Cui).

successful works reported on directly use soft molecular for modification of g-C$_3$N$_4$ [19]. Because the moleculars of soft template are easily to decomposition and restrain the polycondensation of precursors to g-C$_3$N$_4$ during the high-thermal treatment process, which constraints on the structure optimization.

g-C$_3$N$_4$ is a typical organic polymer, which could synthesized from various organic monomers (cyanamide, melamine, urea, etc.). Traced back to ten years ago, soft chemical methods (solvothermal, <400 °C) were often used to synthesize carbon nitride materials. During one-step mobile thermal assembly, g-C$_3$N$_4$ particles with several morphologies were obtained. For example, g-C3N4 sphere was first obtained by Khabashesku et al. through reflux solution reaction of cyanuric chloride and lithium nitride using diglyme as solvent [20]. g-C$_3$N$_4$ nanotube also was synthesized through a catalytic-assembly solvothermal route at 230 °C using cyclohexane as solvent [21]. Solvothermal synthesis of CN based materials in several hot-mediators (DMF, CCl$_4$, triethylamine, benzene, etc.) have been reported, and CN with various structure and morphology could be easily obtained [22–25]. Although the understand of microstructure especially the potential catalytic properties for these products is inadequate, the feasibility for synthesis of g-C$_3$N$_4$ material through hot-liquid mediated process is proved. Also, it is possible to design and modify the molecular stacking structure of g-C$_3$N$_4$ in order to improve the properties in catalytic/photocatalytic field.

In our previous work, wide visible-light responded g-C$_3$N$_4$ nanorod or hollow sphere was successful obtained from solvothermal method without template at 180 °C. Under visible light irradiation, the products could obviously photocatalytic splitting of water to generate hydrogen (6.1 μmol h^{-1}) or decomposition of organic pollutants to small molecules [26,27]. The group of Xu also obtained g-C$_3$N$_4$ sphere through this similar method at 200 °C, but performed none H$_2$ evolution activity without post-treated by calcination [28]. For all this, the photocatalytic activity for g-C$_3$N$_4$ synthesized from low-temperature solvothermal route needs to improved.

In this work, O doped g-C$_3$N$_4$ hollow spheres were first synthesized from acetonitrile solvothermal method at 180 °C. The effect of condensation time to the microstructure and morphology of products was investigated. Various activity tests, like photocatalytic decomposing of dyes, reduction of poisonous metal ions Cr(VI) and producing H$_2$ from water were carried out to evaluate the photocatalytic properties of obtained serious g-C$_3$N$_4$ hollow sphere.

2. Experimental

2.1. Preparation of catalysts

Graphitic carbon nitride hollow microsphere (CNO): The CNO was synthesis by solvothermal synthesis. Typically, 15 mmol cyanuric chloride (CC) and 11 mmol dicyandiamide (DCDA) powders were dispersed in 60 mL acetonitrile. The mixture was stirred for 12 h in a 100 mL Teflon-lined autoclave, and then the autoclave was sealed and maintained at 180 °C for 12–96 h. The obtained products were sequentially washed with distilled water and absolute ethanol several times. After drying at 60 °C for 12 h, products were obtained and defined as CNO-X, where X refers to the condensation time (h).

Pristine g-C$_3$N$_4$ (CNh) was prepared from direct calcination of dicyandiamide at 550 °C for 2 h in air.

2.2. Catalyst characterization

The products were characterized by X-ray diffraction (XRD, D8 Advance) with Cu Ka radiation. The morphology of the samples was explored using a JSM-7001F field-emission scanning electron microscope (FE-SEM) and JEM-2010 high resolution transmission electron microscope (HR-TEM). Fourier transform infrared spectroscopy (FTIR) was recorded from KBr pellets in the range of 400–4000 cm^{-1} on a Nicolet-360 FTIR spectrometer. X-ray photoelectron spectroscopy (XPS) analysis was performed on the ESCALAB 250 photoelectron spectrometer (ThermoFisher Scientific) with Al Ka (1486.6 eV) as the X-ray source set at 100 W and a pass energy of 30 eV for high-resolution scan. UV–vis diffuse reflectance spectra (DRS) were measured With Lambda 750 UV/Vis/NIR spectrophotometer (Perkin-Elmer, USA) using BaSO4 as reference. Photoluminescence (PL) spectra were accomplished in solid with Shimazu RF5301 Spectrofuorophotometer with an excitation wavelength of 413 nm. The solid-state ^{13}C NMR experiment was performed on a Bruker AVANCE III 400 spectrometer.

2.3. Electrochemical analysis

Electrochemical measurements were conducted on a CHI 660E electrochemical workstation with a standard three-electrode cell. An FTO electrode deposited with samples, a platinum wire and saturated Ag/AgCl were employed as the working electrode, counter electrode and reference electrode, respectively. The working electrodes were prepared by drop coating method. The photocurrent and EIS were performed in 0.1 M Na$_2$SO4.

2.4. Measurement of photocatalytic activity

Photocatalytic properties of the products were tested in the decomposition of organic pollutant methyl orange (MO, 10 mg/L), reduction of aqueous Cr(VI) (K$_2$Cr$_2$O$_7$ aqueous solution, 25 mg/L) and hydrogen production. A 300 W Xeon lamp was used as exciting source. Without indication, the photocatalytic reactions were carryout out under visible-light (λ > 420 nm).

Before illumination, 100 mL of MO and Cr(VI) with the addition of 50 mg catalyst was magnetically stirred for 30 min in dark to ensure the adsorption-desorption equilibrium. During illumination, about 4 mL of suspension was taken from the reactor at a scheduled interval. The concentration of MO was determined by absorbance analyse at 464 nm and the contents of Cr(VI) were determined using the diphenylacrbazide colormetric method at 540 nm.

The photocatalytic H$_2$ production was carried out in a Pyrex top-irradiation reaction vessel connected to a glass closed gas system. 50 mg of catalyst power was dispersed in 100 mL aqueous solution containing 10 vol% triethanolamine as sacrificial electron donor. 3 wt% Pt was loaded on the surface of the catalyst by in situ photodeposition method using H$_2$PtCl$_6$ as co-catalyst. Before irradiation, the system was evacuated several times to remove air completely. The temperature of the reaction solution was maintained at 6 °C by the flow of cooling water. The evolved gases were analyzed by gas chromatography equipped with a thermal conductive detector (TCD), using nitrogen as the carrier gas.

3. Results and discussions

3.1. Structural characterization of CNO samples

Fig. 1a presents the XRD patterns of as-prepared CNO catalysts. All materials show an obvious resembled typical g-C$_3$N$_4$ layered structure at 27.4° (d = 0.326 nm) without an impurity phase. This distinct diffraction peak belongs to the long-range inter planar stacking of aromatic systems identified as the (002) peak. Impressively, the intensity of the main (002) peak gradually decreased with the extended condensation time, indicating decreased long-range order of graphitic stacking. Compared to typical graphite XRD pattern of CN material, the peak at ~13° as the (100) peak is not
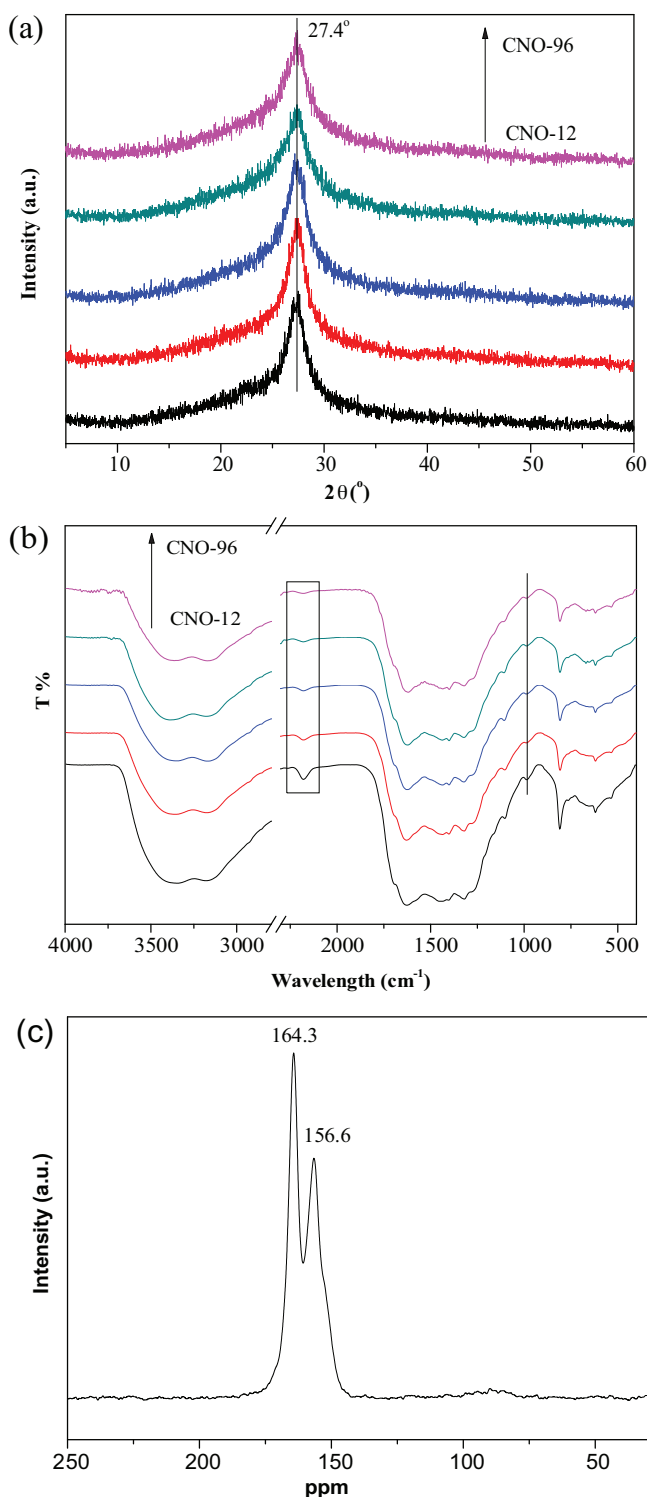
Fig. 1. (a) FTIR spectra, (b) XRD patternn of CNO-samples obtained from different condensation time, and (c) 13C CP-NMR spectrum of CNO-96.

Fig. 2. (a) SEM images for CNO-72, (b, c) CNO-96, (d) TEM images for CNO-96.

The FTIR spectra of the CNO samples synthesized through different times are shown in Fig. 1b. All samples show typical molecular skeletal vibration modes of triazine heterocyclic rings in graphitic carbon nitride. Absorbance in the region of 3200–3400 cm-1 is related to residual symmetric and antisymmetric −NH2 stretching modes and absorbed H2O molecules. A series of bands in the 1200–1700 cm^{-1} region and a strong peak at approximately 810 cm^{-1} are assigned to the stretching vibration of the triazine heterocyclic ring unit and their breathing mode. These bands are very similar to g-C3N4 synthesized from high-temperature polymerization [29]. However, other absorbance peaks can be observed for as-prepared CNO samples. Obviously, a new band at 980 cm^{-1} present in CNO samples, which could be attributed to the stretching modes of N−O groups [30]. It is consistent with the oxygen functionalized carbon nitride reported by Zhang et al. Then, a signal at 2180 cm^{-1} is assigned to the appearance of C≡N, which is not favourable for the formation of network structure of carbon nitride materials [31]. When the condensation time extends, the decreased degree of this disturbed peak indicates the much improved conjugated structure of CNO polymer, even though not completely eliminate.

The proposed heptazine structure was further confirmed by the solid-state 13C cross-polarisation nuclear magnetic resonance (NMR) technology. The spectrum of CNO-96 (Fig. 1c) gives two distinct peaks at 156.6 and 164.3 ppm that can be assigned to the sp2-hybridized carbon atoms of CN2(NHx) and CN3 in the g-C$_3$N$_4$ networks, respectively [32]. The result suggests the presence of characteristic poly(tri-s-triazine) structure in the prepared sample, which is in good agreement with those of bulk g-C$_3$N$_4$ synthesized from high-temperature calcination method [33].

The grain morphology of the products was investigated by SEM and TEM analysis and shown in Figs. 2 and S1. The low magnification SEM image indicates that only irregular particle can be seen in CNO-12. With the condensation time extending, particles with sphere morphology appear, and became more uniform distribution. A conclusion can be reached that the products obtained from this solvothermal process are well-defined microspheres. Clear hollow structure can be observed from broken microsphere and TEM analysis (Fig. 2b, d). The enlarged SEM image (Fig. 2c) reveals that the shell of the hollow microsphere is layered composition which is consistent with XRD. The N2 adsorption–desorption experiments show the surface area of serious samples is about 20 cm^2/g. This low surface area also can be certified from the smooth surface of hollow sphere without any hierarchical porous structure.

observed in as-prepared samples, suggesting the disorder packing of in-plane structural motif, because of the relative lower polymerization degree of carbon nitride than from calcination synthesis at high temperature. This may be attributed to the incomplete molecular polymerization under low temperature. Also, the evolution typical hollow sphere morphology with undulation during the assembly process in liquid medium may disturb the order of layer packing.
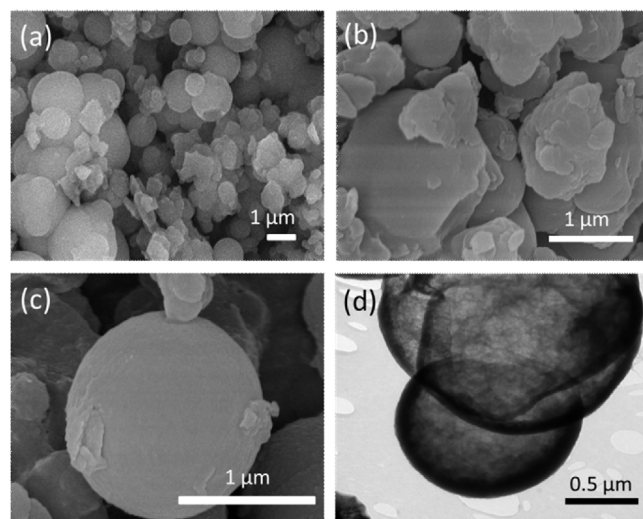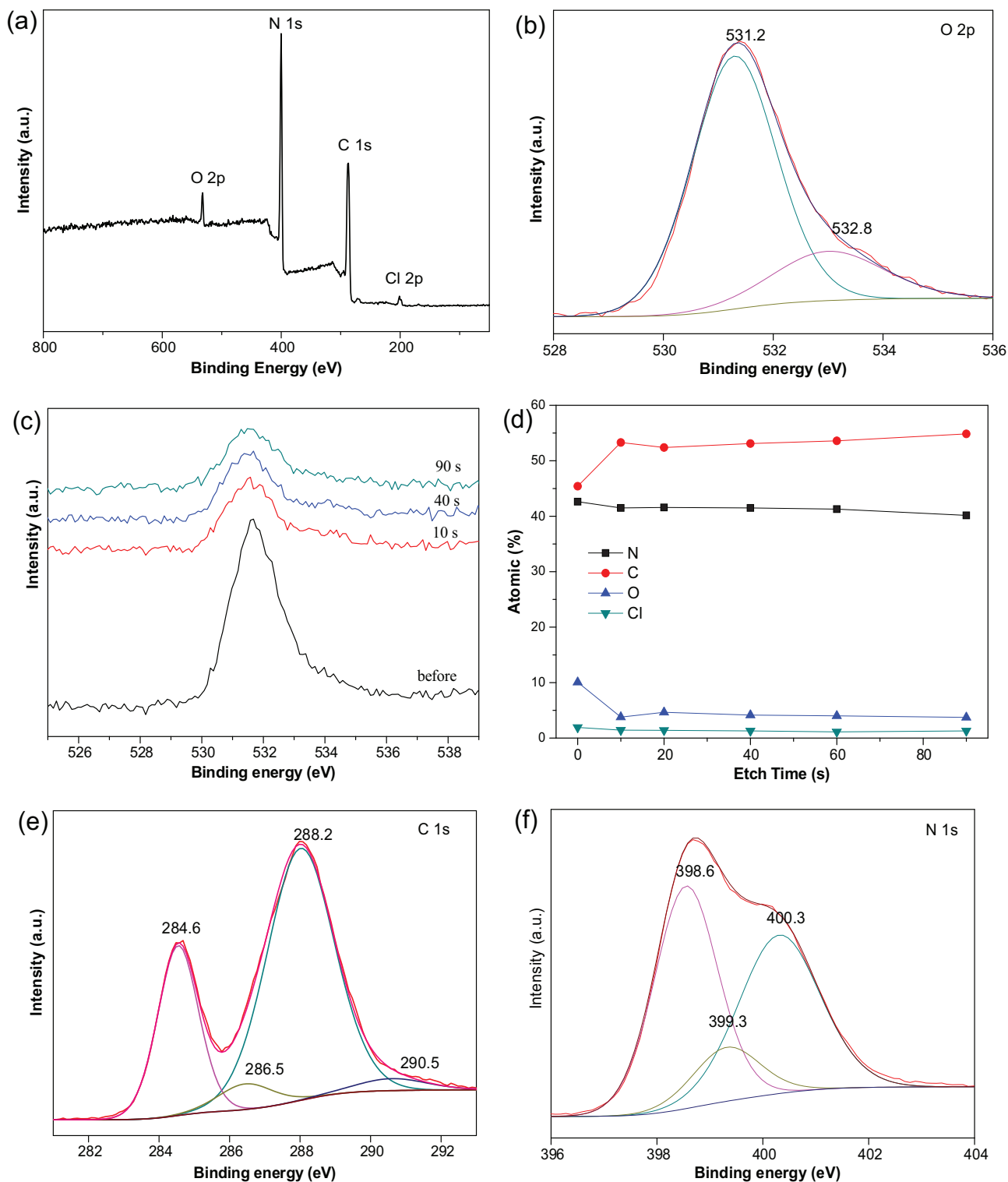
Fig. 3. The XPS of CNO-96 for (a) survey spectrum, (b) O 2p, (e) C 1s, (d) N 1s, (c) O 2p after Ar+ etching, (d) the change of surface atomic after Ar+ etching.

The structure details about oxygen functionalized carbon nitride were further investigated by XPS measurements. Fig. 3 gives the survey and high-resolution XPS spectra of CNO-96. Consistent with various previous reports, serious CNO samples obtained from solvothermal method are mainly composed of C, N, and O elements. The observed Cl 2p signals might be due to some Cl elements in the pores, which could not be easily removed by washing [34]. High-resolution spectra show that the O1s peak can be devolved into two peaks. The O 1s core level at 532.8 eV (O2) could be ascribed to surface adsorbed water [35]. Excitingly, the other core level at 531.2 eV (O1) as the main O component is obviously detected. This signals could be attributed the $C_3-N+-O-$ specie in lattice formed by oxidation of tertiary amines, which is agree with the FTIR results [36]. However, it is difficult to exclude the existence of C—O and N—C—O species in lattice [37].

Table 1
Atom distribution for C, N and O elements derived from the XPS spectra.

Sample	C3/C1	N1/N2	N1/N3	O1/O2
CNO-24	3.8	5.0	1.5	2.2
CNO-48	3.3	4.4	1.4	3.0
CNO-72	2.9	4.0	1.1	4.5
CNO-96	2.5	3.8	1.0	5.4

In order to further verify the functionalized skeleton O, XPS Ar$^+$ etch experiment was performed. After etching for 90 s to remove surface layer, the former disappear but the latter still remain, also the at% of O do not change during 10 s to 90 s etch. This result further suggests the O element is not simply adsorbed on the surface but distributed uniformly in the matrix of sample. No O element contains in synthetic materials, so the O in samples may be derived from O_2 in air introduced during pre-treatment. Under subcritical hot-fluid conditions, the O_2 molecular was activated and embedded into the heterocyclic structure of CN polymer.

The C 1s spectra (Fig. 3e) can be separated into four peaks, C1 (284.6 eV) in sp2 C—C bonds, C2 (286.5 eV) in C—NH$_2$ species, C3 (288.2 eV) in sp2-hybridized carbon in N-containing aromatic ring N—C—N. A weak peak at 290.5 eV (C4) confirms the formation of C—O bond [38]. N1s XPS spectrum exhibits pyridinic nitrogen N1 (C=N—C, 398.6 eV), sp bonded nitrogen in the terminal C≡N groups from the unreacted nitrile groups N2 (399.3 eV) or bridging N atoms in amino groups (C—N—H), and bridge N in N—[C]3 N3 (400.3 eV).

Detail XPS investigation were also applied for samples obtained during different condensation time. Results are shown in Fig. S2. All samples possess similar chemical bonding of C/N/O elements. But the relatively atomic ratio of N1:N3 and C3: C1, which can express the existence of sp2 hybrid triazine-based structure gradually decrease from 5.0 to 3.85 and 3.8 to 2.5. Meanwhile, the concentration of C1 is obvious increase from CN-24 to CN-96 (Table 1). These results indicate that the extended condensation time bring to sp2 C—N bonds translate into graphitic C, therefore, cause the imperfection of polymerization structure. The increased defects in this hollow structure may conducive to the light-harvesting and mass transfer. In addition, the atomic ratio of O1:O2 increase from 2.2 to 5.3, which indicates the increasing doped O. During subcritical condition, extending reaction time makes for more active O atom embed into the skeleton of carbon nitride framework.

In short summary, according to the aforementioned analysis results, we can conclude that the O functionalized hollow sphere carbon nitride materials with imperfect heptazine structure were fairly obtained from one-step solvothermal route without template.

3.2. Photoelectric properties of CNO samples

The optical absorption and energy band gap of CNO samples are greatly altered by the solvothermal condensation time, as shown by the UV–vis diffuse reflectance spectroscopy (DRS) (Fig. 4a). Considerable improved light-harvesting capability across the whole DRS and gradual bathochromic shift of optical absorption edges are found for samples prepared under extending condensation time. The absorption band edge of samples red shift from approximately 550–680 nm and the electronic band gap determined from the Tauc plot narrowed from 2.29 to 1.87 eV for CNO-12 to CNO-96. The modified light-absorption mainly owing to the improved p-electron delocalization and inter-planar packing towards J-type aggregates in the conjugated system from solvothermal processing. Meanwhile, the reduced C—N bond length by O-doping would narrow the band gap of the materials [37].

To confirm the band structure, valence-band XPS was carried out to analyse the valence band (VB) potential (Fig. 4b). For CNO-48
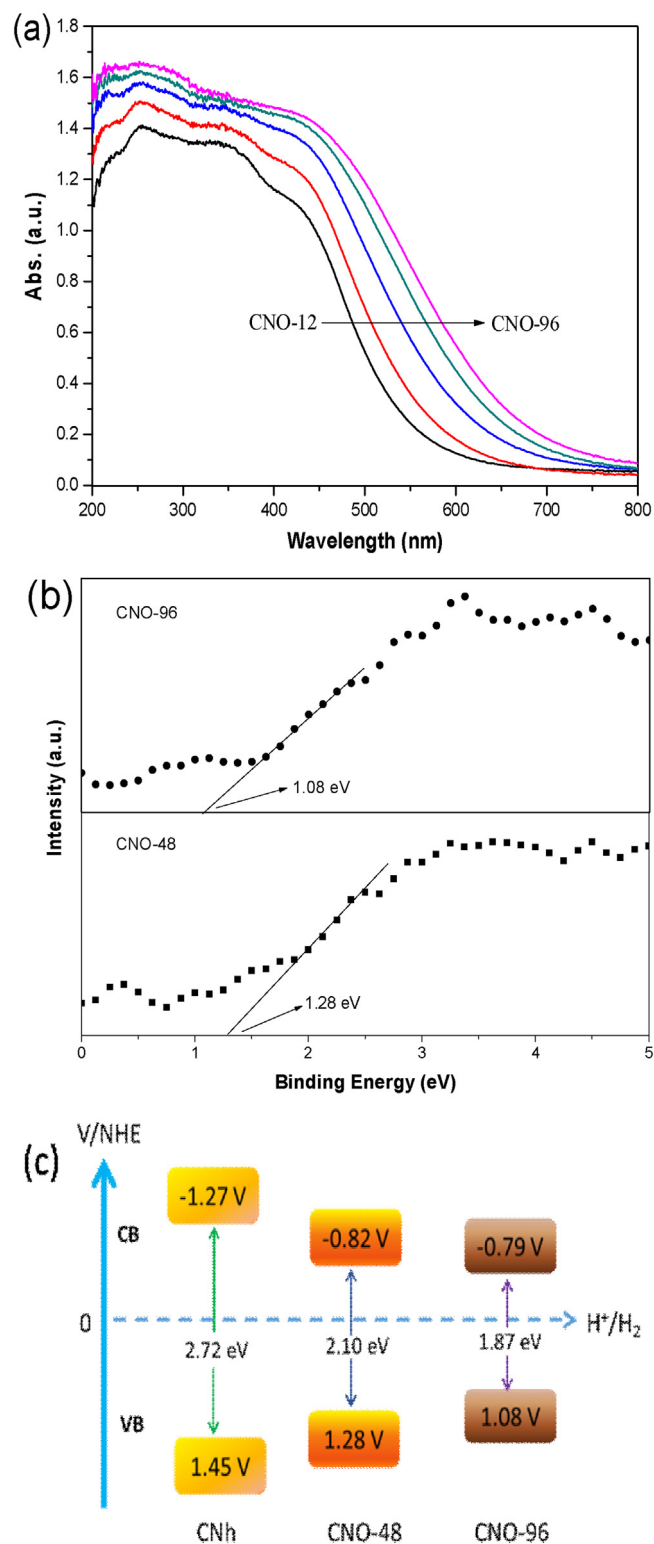

Fig. 4. UV–vis adsorption spectra of CNO samples, (b) The XPS valence band spectra of CNO-48 and CNO-96, (c) Schematic illustration of the determined CB and VB edges of samples, (d) Room-temperature PL spectra of CNO samples.

and CNO-96, the VB potentials are 1.28 eV and 1.08 eV, respectively, which are higher than that of pristine g-C$_3$N$_4$ (1.44 eV, Fig. S3). Combined with their band gap, the conduction band (CB) level can be deduced, and the determined relative CB and VB edges of samples for pristine g-C$_3$N$_4$, CNO-48 and CNO-96 are illustrated in Fig. 4c. It is clear that the electronic structure of CNO samples can be
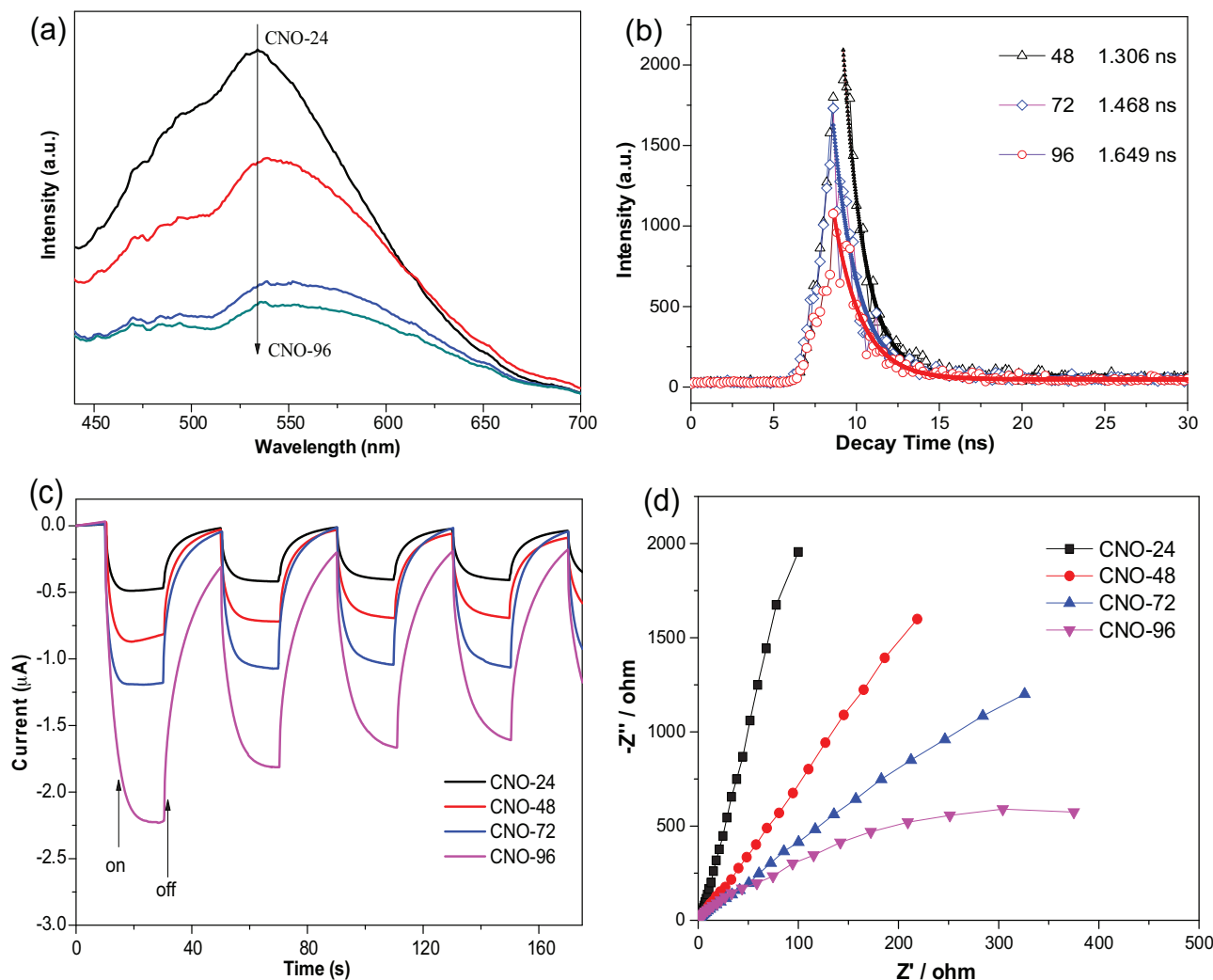
Fig. 5. (a) Room-temperature PL spectra, (b) Time-resolved PL spectra, (c) Electrochemical impedance spectra, and (d) Photocurrent under visible light ($\lambda > 420$ nm) in pH 7.0 Na_2SO_4 solution of CNO samples.

tailored just from condensation parameters adjustment. With the prolonged condensation time, the VB edges increase and the CB edges decrease. The narrowed band gap of CNO samples could be ascribed to the introduction of O atoms and graphitic C, which may extend the delocalized p-electron system [39,40]. It is beneficial to reduce the exciting energy of photocatalysts, therefore, greatly improving the light efficiency. Meanwhile, these results show that CNO samples thermodynamically enable photocatalytic reduction of water into H_2 and purification of environmental pollutants, even though the CB potential are little lower than that of CNh.

For this O-doped hollow CNO samples, enhanced light-harvesting and narrowed band gap have been achieved. However, whether this materials could perform improved photocatalytic activity or not? To answer this question, the combined techniques of steady-state and time-resolved PL spectroscopy, as well as electrochemical tests were employed to investigate the charge separation and transfer behaviours in CNO.

In Fig. 5a, with 413 nm light excitation, a broad visible PL band located at about 550 nm can be found for the CNO samples, indicating that electron–hole pairs can be produced upon absorbing photons, which is a crucial step to initiate the photocatalytic reaction. This energy-wasteful process can be greatly suppressed for samples obtained from extending condensation time, which indicates a suppressed recombination rate of the photo-induced charge

carriers. In addition, the PL peak of CNO-96 slightly redshift compared to CNO-24, which gives an indication that larger conjugated ring structures are present [41].

The fitting decay spectra and the radiative lifetimes of CNO samples are shown in Fig. 5b. The lifetimes of the carriers were determined to be 1.31–1.65 ns for CNO-48 to CNO-96, indicating that the modified electron-hole pairs transferring effective was achieved.

The photocurrent responses (Fig. 5c) indicated that the photo-induced electron density of CNO samples was in order of CNO–96 > CNO–72 > CNO–48 > CNO-24. Consistently, CNO-96 has lower resistance in electron transport in the electrochemical impedance spectra (Fig. 5d). These results imply that the O-doping hollow structures of CNO improve the transport of photogenerated charge carriers from inside to surface and thereby enhance the photocatalytic activities.

Considering the aforementioned light harvesting capability and charge separation efficiency, the photocatalytic performance is predicted as follows: CNO–96 > CNO–72 > CNO–48 > CNO-24.

3.3. Photocatalytic performance and mechanism of CNO samples

The phtocatytic performance of CNO samples for water treatment by degradation of organic pollutants MO and reduction of
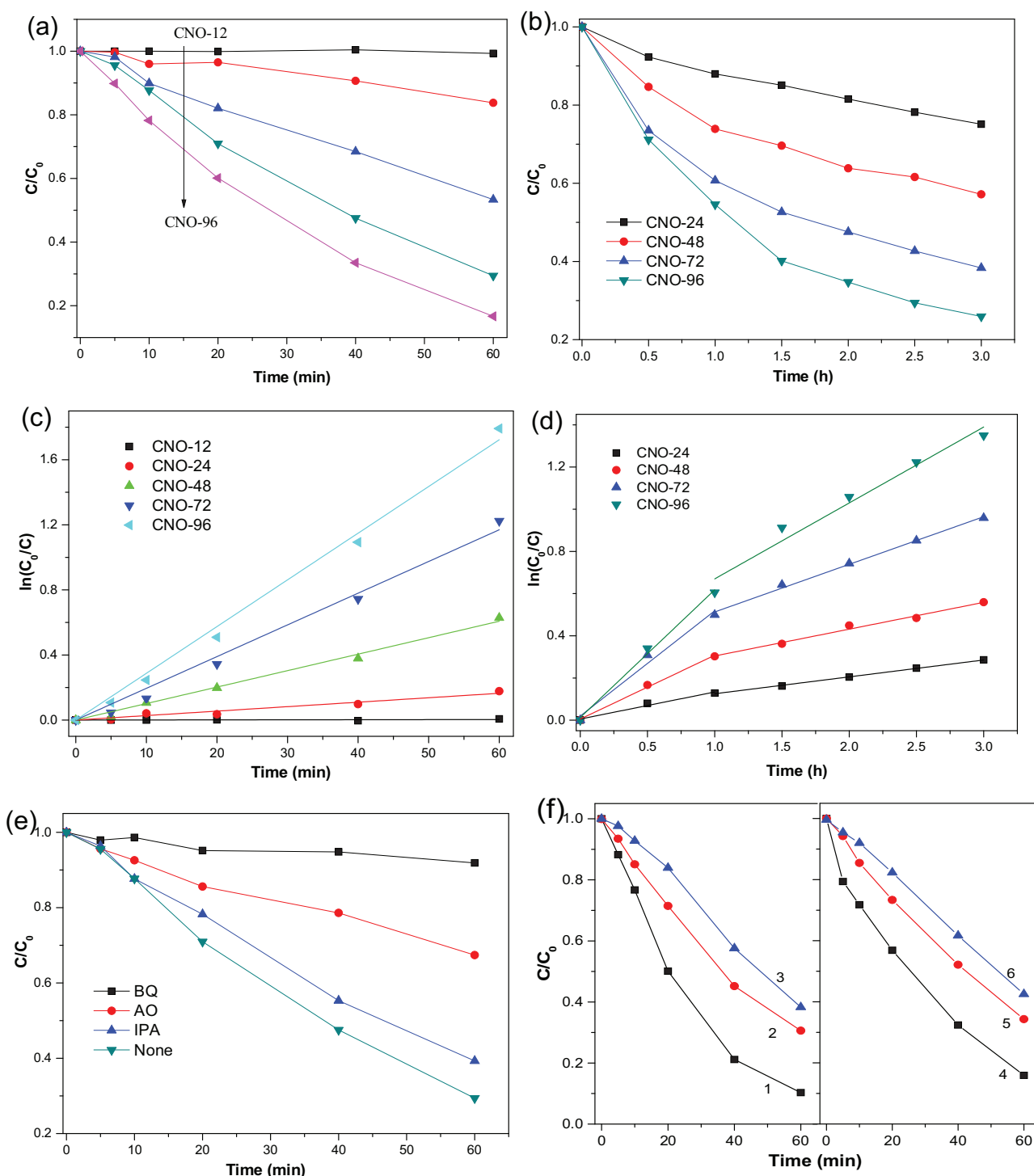
Fig. 6. (a) Photocatalytic activity for degradation of MO and (b) Reduction of Cr(VI) under visible light irradiation (λ > 420 nm), (c,d)The corresponding reaction kinetic fitted curves, (e) Effect of on the degradation of MO on CNO-96, (f) Cycling runs for the degradation of MO over CNO-96.

aqueous Cr(VI) as a function of reaction time is shown in Fig. 6a,b. The effect of adsorption and photolysis of reactant are excluded by controlled experiments (Fig. S4). Obviously, CNO with hollow sphere morphology synthesized from one-step solvothermal method could photocatalytic treatment of environmental pollutant effectively. The synthetic time greatly influences the photocatalytic performance of obtained CNO materials, and CNO-96 exhibits the highest activity. After light illumination for an hour, more than 80% of MO was bleached by CNO-96. The similar trend can be seen for

Cr(VI) reduction, and more than 75% of the Cr(VI) was reduced after light illumination for 3 h.

The pseudo-first order reaction kinetic model is adopted for fitting the reaction process for both MO degradation and Cr(VI) reduction on CNO samples and the results demonstrate the linear relationship well. The curves of $\ln(C_0/C)$ as a function of irradiation time are shown in Fig. 6c,d and the calculated degradation rate constants are provided in Table 2. During Cr(VI) reduction process, two-stage kinetics process can be seen for CNO-48 to CNO-96, and

Table 2
Physicochemical properties and photocataltic activity of CNO samples.

Sample	C/N Atomic	Eg (Ev)	K		HER	
			MO (10^2 min^{-1})	Cr(VI) (10 h^{-1})	Vis (μmol h^{-1})	Uv + Vis
CNO-24	0.63	2.21	0.27	1.3	9.1	9.3
CNO-48	0.62	2.10	1.0	3.0	10.4	11.4
CNO-72	0.63	1.97	1.9	5.0	11.7	12.6
CNO-96	0.66	1.87	2.9	6.1	13.2	17.4

after irradiated for 1 h, the reaction rate slightly decrease. This may be due to the reduced Cr(III) species deposited on the surface of materials which occupied the active sites and reduce he reaction rate [42,43].

In order to demonstrate the mechanism for the photocatalytic water treatment over CNO samples, the scavengers p-benzoquinone (BQ), isopropanol (IPA) and ammonium oxalate (AO) were added to quench the possible active species $\bullet O_2{}^-$, $\bullet OH$ and h$^+$ during degradation of MO over CNO-96. As shown in Fig. 6e, when IPA was added, the remoal rate of MO had no obvious decrease, implying that $\bullet OH$ did not dominate the photocatalytic reaction. However, dramatic decline of MO removal was achieved in the preaence of BQ, suggesting that $\bullet O_2{}^-$ was the main active species. h+ was also participate in partial reaction. This result is coincident with the energy band structure of CNO-96 concluded by above analysis.

The stability of the photocatalyst is crucial for application in aqueous solution. To confirm the possibility of recycling of the obtained CNO samples, recycling experiments were performed with CNO-96 in the degradation of MO (Fig. 6f). After 3 runs, although the MO removal rate slight decreased, it mainly caused from the mass loss (about 20 mg) of catalysts. After corresponding catalyst supplement in run 4, the degradation rate was recovered. Therefore, CNO-96 can maintain a certain degree of activity stability during water purification.

To further investigate the photocatalytic property for this novel CNO hollow spheres, photocatalytic splitting of water for H_2 production reaction was carried out in aqueous solution with TEOA (10 vol%) as sacrificial agent and 3 wt% Pt as a co-catalyst. Pt is in situ photodeposited on photocatalysts. As shown in Fig. 7a, the H_2 yield in the first 1 h irradiation is increased for samples obtained from longer condensation time. The CNO-96 showed highest H_2 generation yield (13.2 μmol) under visible light irradiation (780 nm > λ > 400 nm), which is even 1.5 times higher than that (9.05 μmol) over CNO-24. Moreover, the photocatalytic activity of all samples were obviously enhanced, when the irradiation light expanded to UV-light (1100 nm > λ > 300 nm). About 17.4 μmol H_2 was detected during initial 1 h irradiation for CNO-96.

Compared to so many reports about g-C_3N_4 for photocatalytic application, the H_2 evolution rate about these samples was not competitive [44,45]. However, for g-C_3N_4 synthesized from solvothermal route under low temperature, it is still a great progress. Control experiments for H_2 evolution test on bulk g-C_3N_4 obtained from DCDA direct calcination (500–600 °C) was done, and results are shown in Fig. S5. In the same reaction system, 16.2 μmol H_2 can be detected for bulk samples even synthesized at 600 °C. The results thus underline the positive role and infinite potential of solvothermal synthesis of CN-based semiconductor at low temperature.

The sustaining photocatalytic H_2 evolution activity over CNO-96 photocatalyst was also evaluated by continuous irradiation under the same visible light condition. As shown in Fig. 7b, continuous H_2 production can be detected and no obvious activity loss was observed after 10 h reactions, revealing the relative excellent stability of the CNO-samples for H_2 evolution.
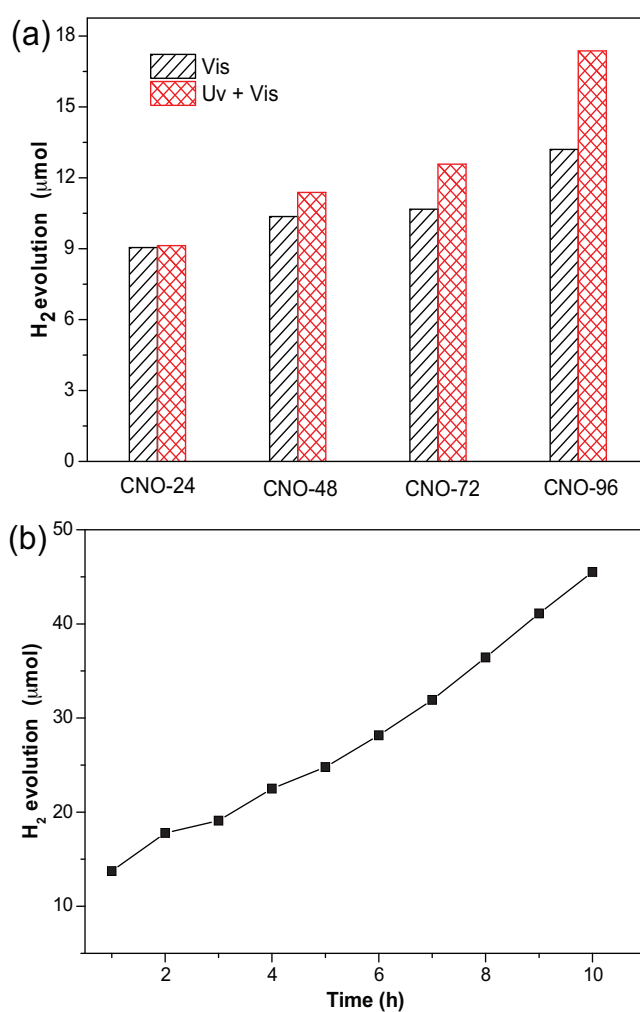

Fig. 7. (a) The photocatalytic hydrogen evolution at the initial 1 h irradiation over CNO samples, (b) The sustaining photocatalytic hydrogen evolution over CNO-96 under visible light (λ > 420 nm).

The structure and morphology investigation results for used samples were characterized by FTIR and SEM, shown in Fig. S6. After photocatalytic reaction for decomposition of environmental pollutants and splitting water for H_2 evolution, nearly same features of hybrid C—N conjugate skeleton and sphere morphology with almost no change can be found. This result indicates that the CNO hollow sphere photocatalyst has very good stability during the photocatalytic reaction.

4. Conclusion

In summary, O-doped graphitic carbon nitride with hollow sphere particle morphology CNO was successfully synthesized by a facile "one-pot" solvothermal approach. The O species doped

into the lattice of heptazine heterocyclic ring were derived from oxygen molecular activated during pressure-tight subcritical conditions. Appropriate solvothermal condensation time avail O doping content and energy band regulation. Due to the optimized delocalization network and heteroelements doping, the visible light response was enhanced and the separation efficiency of the photoinduced charge carriers was improved. As a result, this novel material shows remarkably photocatalytic activity for organic molecular degradation and toxic heavy metal ions reduction. Significant effect for H_2 evolution from water splitting under light irradiation was also achieved. This work demonstrates a facile strategy to synthesize and tailor the structure and morphology of g-C_3N_4 based materials under mild conditions, therefor to offer a reference way for fabricating highly efficient non-metal photocatalysts.

Acknowledgments

Appendix A. Supplementary data

Supplementary data associated with this article can be found, in the online version, at http://dx.doi.org/10.1016/j.apcatb.2017.01.041.

References

[1] A. Mills, R.H. Davies, D. Worsley, Chem. Soc. Rev. 22 (1993) 417–425.
[2] X.J. Lang, X.D. Chen, J.C. Zhao, Chem. Soc. Rev. 43 (2014) 473–486.
[3] X.B. Chen, S.H. Shen, L.J. Guo, S.S. Mao, Chem. Rev. 110 (2010) 6503–6570.
[4] J.H. Park, F. Raza, S.J. Jeon, D.B. Yim, H.I. Kim, T.W. Kang, J.H. Kim, J. Mater. Chem. A 4 (2016) 14796–14803.
[5] J. Li, Y. Yu, L.Z. Zhang, Nanoscale 6 (2014) 8473–8488.
[6] X.Q. Yan, C. Xue, B.L. Yang, G.D. Yang, Appl. Surf. Sci. 394 (2017) 248–257.
[7] X.C. Wang, K. Maeda, A. Thomas, K. Takanabe, G. Xin, J.M. Carlsson, K. Domen, M. Antonietti, Nat. Mater. 8 (2008) 76–80.
[8] W.J. Ong, L.L. Tan, Y.H. Ng, S.T. Yong, S.P. Chai, Chem. Rev. 116 (2016) 7159–7329.
[9] K. Maeda, K. Sekizawaa, O. Ishitani, Chem. Commun. 49 (2013) 10127–10129.
[10] S.W. Cao, J.X. Low, J.G. Yu, M. Jaroniec, Adv. Mater. 27 (2015) 2150–2176.
[11] B. Lin, G.D. Yang, B.L. Yang, Y.X. Zhao, Appl. Catal. B: Environ. 198 (2016) 276–285.
[12] C.B. Lin, C. Xue, X.Q. Yan, G.D. Yang, G. Yang, B.L. Yang, Appl. Surf. Sci. 357 (2015) 346–355.
[13] X.C. Wang, K. Maeda, X.F. Chen, K. Takanabe, K. Domen, Y.D. Hou, X.Z. Fu, M. Antonietti, J. Am. Chem. Soc. 131 (2009) 1680–1681.
[14] Y.J. Cui, J.S. Zhang, G.G. Zhang, J.H. Huang, P. Liu, M. Antonietti, X.C. Wang, J. Mater. Chem. 21 (2011) 13032–13039.
[15] J. Liu, J.H. Huang, H. Zhou, M. Antonietti, ACS Appl. Mater. Interfaces 6 (2014) 8434–8440.
[16] J.H. Huang, M. Antonietti, J. Liu, J. Mater. Chem. A 2 (2014) 7686–7693.
[17] Y. Zheng, L.H. Lin, B. Wang, X.C. Wang, Angew. Chem. Int. Ed. 54 (2015) 12868–12884.
[18] J. Xu, Y.J. Wang, Y.F. Zhu, Langmuir 29 (2013) 10566–10572.
[19] Y. Wang, X.C. Wang, M. Antonietti, Y.J. Zhang, ChemSusChem 3 (2010) 435–439.
[20] J.L. Zimmerman, R. Williams, V.N. Khabashesku, J.L. Margrave, Nano Lett. 1 (2001) 731–734.
[21] C.B. Cao, F.L. Huang, C.T. Cao, J. Li, H.S. Zhu, Chem. Mater. 16 (2004) 5213–5215.
[22] Q.X. Guo, Y. Xie, X.J. Wang, S.C. Lv, T. Hou, X.M. Liu, Chem. Phys. Lett. 380 (2003) 84–87.
[23] X.F. Lu, L.G. Gai, D.L. Cui, H.H. Jiang, Q.L. Wang, X. Zhao, X.T. Tao, M.H. Jiang, J. Cryst. Growth 306 (2007) 400–405.
[24] J. Zhang, W. Liu, X.F. Li, B.Q. Zhan, Q.L. Cui, G.T. Zou, Mater. Res. Bull. 44 (2009) 294–297.
[25] G. Demazeau, J. Mater. Chem. 9 (1999) 15–18.
[26] Y.J. Cui, Z.X. Ding, X.Z. Fu, X.C. Wang, Angew. Chem. Int. Ed. 51 (2012) 11814–11818.
[27] Y.J. Cui, Y.B. Tang, X.C. Wang, Mater. Lett. 161 (2015) 197–200.
[28] Q. Gu, Y.S. Liao, L.S. Yin, J.L. Long, X.X. Wang, C. Xue, Appl. Catal. B: Environ. 165 (2015) 503–510.
[29] Y.J. Cui, Z.X. Ding, P. Liu, M. Antonietti, X.Z. Fu, X.C. Wang, Phys. Chem. Chem. Phys. 14 (2012) 1455–1462.
[30] T.S. Kurtikyan, S.R. Eksuzyan, V.A. Hayrapetyan, G.G. Martirosyan, G.S. Hovhannisyan, G.A. Goodwin, J. Am. Chem. Soc. 134 (2012) 13861–13870.
[31] G.H. Dong, Z.H. Ai, L.Z. Zhang, RSC Adv. 4 (2014) 5553–5556.
[32] Y.S. Fu, J.W. Zhu, C. Hu, X.D. Wu, X. Wang, Nanoscale 6 (2014) 12555–12564.
[33] J.S. Zhang, G.G. Zhang, X.F. Chen, S. Lin, L. Möhlmann, G. Dołęga, G. Lipner, M. Antonietti, S. Blechert, X.C. Wang, Angew. Chem. Int. Ed. 51 (2012) 3183–3187.
[34] K. Kailasam, J. Schmidt, H. Bildirir, G.G. Zhang, S. Blechert, X.C. Wang, A. Thomas, Macromol. Rapid Commun. 34 (2013) 1008–1013.
[35] Y.X. Li, H. Xu, S.X. Ouyang, D. Lu, X. Wang, D.F. Wang, J.H. Ye, J. Mater. Chem. A 4 (2016) 2943–2950.
[36] D.A. Dobrzanska, A.L. Cooper, C.G. Dowson, S.D. Evans, D.G. Fox, B.R. Johnson, C.I. Biggs, R.K. Randev, H.M. Stec, P.C. Taylor, A. Marsh, Langmuir 29 (2013) 2961–2970.
[37] Z.F. Huang, J.J. Song, L. Pan, Z.M. Wang, X.Q. Zhang, J.J. Zou, W.B. Mi, X.W. Zhang, L. Wang, Nano Energy 12 (2015) 646–656.
[38] J.H. Li, B. Shen, Z.H. Hong, B.Z. Lin, B.F. Gao, Y.L. Chen, Chem. Commun. 48 (2012) 12017–12019.
[39] Y.B. Ding, Y.H. Tang, L.M. Yang, Y.X. Zeng, J.L. Yuan, T. Liu, S.Q. Zhang, C.B. Liu, S.L. Luo, J. Mater. Chem. A 4 (2016) 14307–14315.
[40] W.L. Yang, L. Zhang, J.F. Xie, X.D. Zhang, Q.H. Liu, T. Yao, S.Q. Wei, Q. Zhang, Y. Xie, Angew. Chem. Int. Ed. 55 (2016) 6716–6720.
[41] A. Thomas, A. Fischer, F. Goettmann, M. Antonietti, J.O. Müller, R.S.J.M. Carlsson, J. Mater. Chem. 18 (2008) 4893–4908.
[42] Y.C. Zhang, Q. Zhang, Q.W. Shi, Z.Y. Cai, Z.J. Yang, Sep. Purif. Technol. 142 (2015) 251–257.
[43] X.F. Hu, H.H. Ji, F. Chang, Y.M. Luo, Catal.Today 224 (2014) 34–40.
[44] F. He, G. Chen, Y.S. Zhou, Y.G. Yu, Y. Zheng, S. Hao, Chem. Commun. 51 (2015) 16244–16246.
[45] Y. Zheng, L.H. Lin, X.J. Ye, F.S. Guo, X.C. Wang, Angew. Chem. Int. Ed. 53 (2014) 11926–11930.